PHYSICAL REVIEW B VOLUME 60, NUMBER 2 1 JULY 1999-II

Grain-boundary magnetoresistance in manganites: Spin-polarized inelastic tunneling through a spin-glass-like barrier

M. Ziese
Department of Physics and Astronomy, University of Sheffield, Sheffield S3 7RH, United Kingdom
(Received 6 January 1999)

The grain-boundary magnetoresistance of various $La_{0.7}Ca_{0.3}MnO_3$ samples was investigated by resistance, magnetoresistance, and dynamic conductance measurements. Data on five samples, namely an epitaxial film, a polycrystalline film, a step-edge array, a mechanically induced grain boundary, and a chromium-manganite tunneling contact, are presented. A model of spin-polarized inelastic tunneling through an insulating barrier with spin-glass-like characteristics is proposed that explains the experimental observations.
[S0163-1829(99)50926-0]

It was experimentally observed that polycrystalline and single crystalline manganite samples of the type $La_{0.7}Ca_{0.3}MnO_3$ (LCMO) show significantly different magnetoresistance characteristics.[1,2] Whereas the magnetoresistance of single crystals or epitaxial films varies slowly in small magnetic fields, a steep decrease in the magnetoresistance is seen at low fields for polycrystalline films and ceramics. This behavior was tentatively interpreted as spin-polarized tunneling through an insulating layer separating ferromagnetic grains with high spin polarization.[1,3] The polycrystalline samples show certain reproducible features, namely a linear magnetic field dependence of the resistance in the high-field limit,[1] a strong decrease of the low-field magnetoresistance with temperature, and an anisotropic magnetoresistance.[4,5] Evetts *et al.*[4] pointed out that the grain-boundary region is likely to be magnetic and they developed a model based on magnetic polarization of the grain boundary by the adjacent ferromagnetic grains. Recently Balcells *et al.*[6] showed that the tunneling barrier is a noncollinear ferromagnet. Conclusive information about the transport mechanism, however, can only be obtained from dynamic conductance measurements. In this work, resistance, magnetoresistance and, most important, dynamic conductance measurements on various samples are presented and analyzed. The data can be understood within a model of inelastic tunneling between ferromagnetic regions through a spin-glass-like barrier.

Five samples were investigated here. A 200 nm thick LCMO film on $LaAlO_3$ (sample S1) was used as a reference sample. The characteristics of few grain boundaries could be favorably investigated on a step-edge array (S2) containing 200 steps along [110] of height 140 nm and 20 μm apart,[7] as well as on a mechanically induced grain boundary (S3) along [100].[8] These samples had thicknesses of 25 nm and 20 nm, respectively. For comparison, a 250 nm thick polycrystalline LCMO film on MgO (S4) was measured. From TEM images of similar samples, the grain size of film S4 was estimated to be about 100 nm. Mieville *et al.* showed that some metal-manganite contacts have tunneling characteristics.[9] Since the transport mechanism in these contacts is supposed to be similar to the transport through grain boundaries, a Cr-LCMO contact (S5) was studied here. Sample S5 consisted of a LCMO bridge 185 μm wide and 1.8 mm long with three chromium contacts of dimension 185 μm by 185 μm; it was measured in three point geometry, whereas the other samples were measured in the standard four point geometry. The resistance and magnetoresistance of the Cr-LCMO contact was approximated by the difference of measurements taken at low (30 mV) and high (3 V) voltages. All LCMO films were deposited from a stoichiometric target on $LaAlO_3$ (001) and MgO (001) substrates by pulsed laser ablation. During the deposition process the substrates were heated to about 650 °C; the oxygen pressure in the chamber was 100 mTorr. The Curie temperatures T_C measured magnetically were 224.0 K (S1), 208 K (S2), 212 K (S3), and 218.6 K (S4). The zero-field resistance is shown in Fig. 1. The measurements were performed in the linear regime for samples S1, S2, and S4, whereas the resistance of sample S3 was recorded in the nonlinear regime at 1 V (S3).

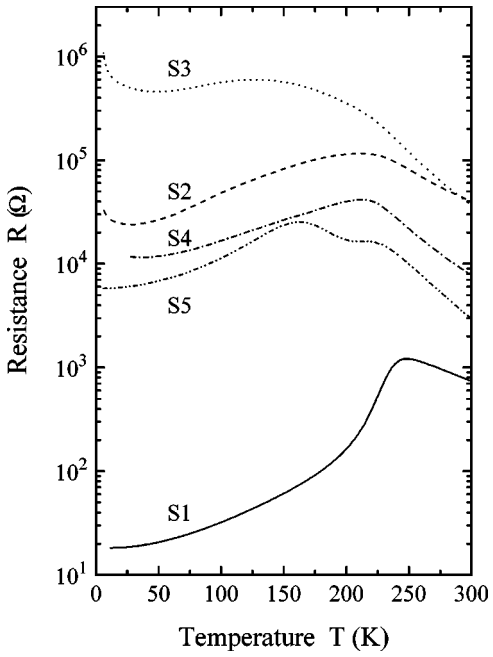

FIG. 1. Zero-field resistance of the investigated samples as a function of temperature.

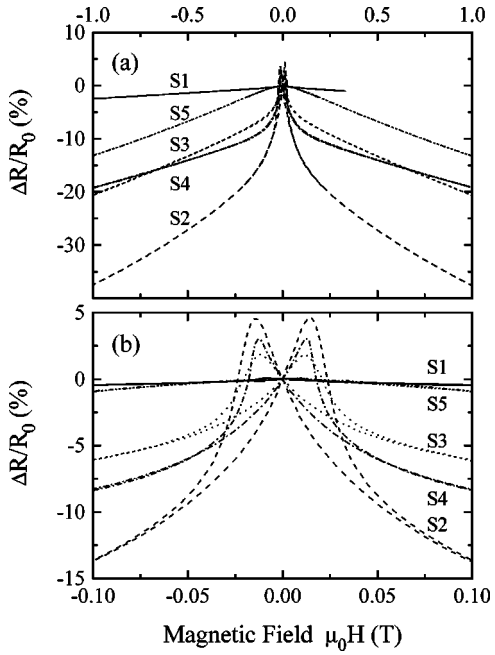

FIG. 2. Magnetoresistance ratio $\Delta R/R_0$ of the investigated samples at 100 K in the (a) high-field regime and (b) low-field regime.

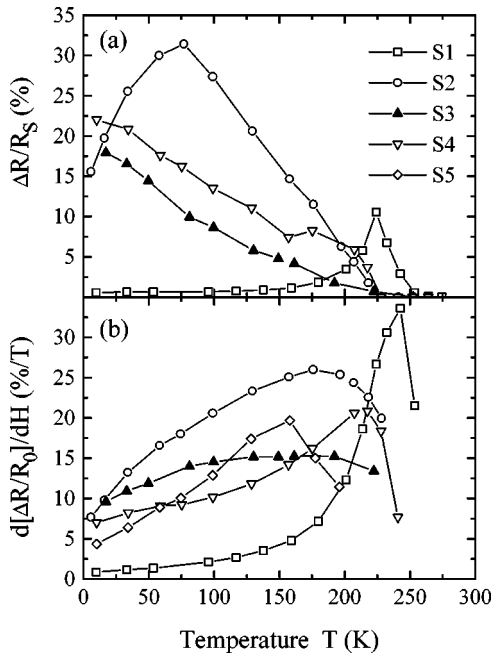

FIG. 3. (a) Low-field magnetoresistance $\Delta R/R_S$ [see Eq. (1)] and (b) high-field slope $d[\Delta R/R_0]/dH$ as a function of temperature.

The magnetoresistance ratio $\Delta R/R_0=[R(H)-R_0]/R_0$ at 100 K is shown in the (a) high-field regime and (b) low-field regime in Figs. 2(a) and (b). Samples S2, S3, and S4 show a considerable low-field magnetoresistance; the magnetoresistance of all samples is linear in high magnetic fields. R_0 denotes the zero-field resistance after field cycling from 1 to 0 T. The two magnetoresistance regimes correspond to the alignment of the magnetically soft grains at low fields and the intrinsic barrier magnetoresistance at high fields. The steep resistance decrease in low fields is absent in the Cr-LCMO contact, since only one electrode is ferromagnetic. In this case the barrier is likely to consist of an oxygen depleted LCMO layer as well as a chromium-oxide layer. An effective zero-field resistance R_S was obtained for samples S2–S4 by extrapolation of the linear high-field magnetoresistance to zero. Accordingly the low-field magnetoresistance was defined by

$$\Delta R/R_S=[R_{max}-R_S]/R_S, \tag{1}$$

where R_{max} denotes the maximal resistance. This low-field magnetoresistance and the high-field magnetoresistance slope $d[\Delta R/R_0]/dH$ are shown in Fig. 3. For comparison an effective low-field magnetoresistance was defined for the epitaxial film S1 by $\Delta R/R_S=[R_{max}-R(H)]/R_0$ with $\mu_0 H=0.1$ T. Both the low-field magnetoresistance and the high-field magnetoresistance slope of the epitaxial film are sharply peaked near the Curie temperature and have a temperature dependence significantly different from the other samples.

Current-voltage characteristics were measured for all samples and were used to calculate the dynamic conductance $G=dI/dV$. The I-V characteristics of the epitaxial film S1 were linear within 0.05% in the investigated temperature $T \leqslant 150$ K and voltage range $V<30$ mV, whereas samples S2–S5 show nonlinear current-voltage characteristics. Typical conductance curves of samples S2, S3, and S5 recorded at 100 K in zero magnetic field are shown in Fig. 4; the nonlinear conductance observed for the polycrystalline film S4 was small $<1\%$. The shape of the conductance curves did not depend on the applied field. All samples showed nonquadratic dependences at this temperature. The measured conductance was analyzed with the expression

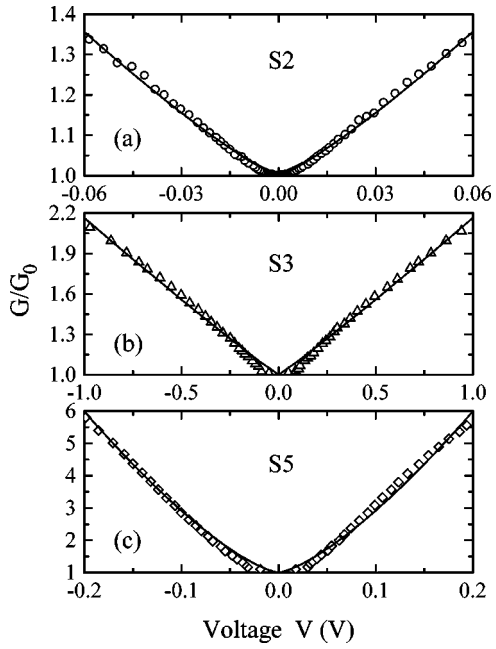

FIG. 4. Dynamic conductance $G=dI/dV$ as a function of applied voltage for (a) the step-edge array (S2), (b) the mechanically induced grain boundary (S3), and (c) the Cr-LCMO contact (S5) at 100 K in zero magnetic field. The conductance is plotted versus (a) the voltage drop per step, (b) the voltage drop over the disordered region, and (c) the voltage drop over the barrier. The solid lines are fits of Eq. (2) to the data.

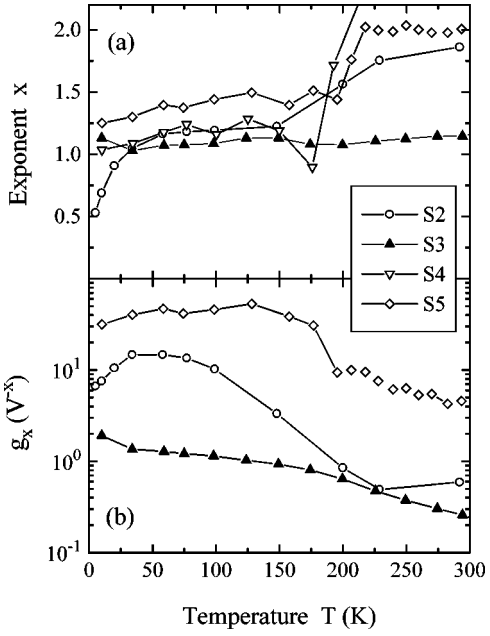

FIG. 5. (a) Dynamic conductance exponent x and (b) nonlinear conductance g_x defined by Eq. (2) for samples S2–S5.

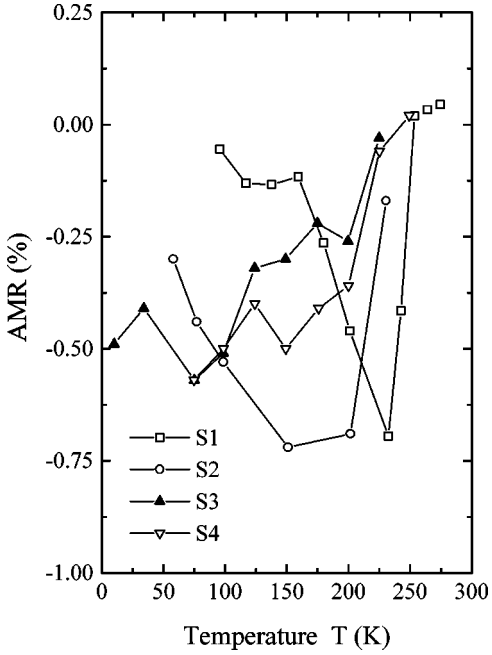

FIG. 6. Anisotropic magnetoresistance ratio (AMR) [see Eq. (3)] as a function of temperature.

$$G/G_0 = 1 + g_x V^x \tag{2}$$

that is suggested by inelastic tunneling studies.[10] G_0 denotes the conductance in the zero voltage limit. Fits of Eq. (2) to the data yielded the conductance exponent x and the nonlinear conductance g_x, both shown in Fig. 5. The exponent x is nearly temperature independent for the mechanically induced grain boundary S3, whereas samples S2, S4, and S5 show a crossover from a low temperature value of $x \sim 1.2-1.4$ to a high temperature value ~ 2 corresponding to the direct tunneling limit.[11] Furthermore the step-edge array S2 shows a strongly decreasing value of x below about 50 K corresponding to the decrease in the low-field magnetoresistance in this temperature range. In studies of $YBa_2Cu_3O_7$/LCMO/$YBa_2Cu_3O_7$ trilayers a value $x = 4/3$ was found[12] in agreement with inelastic tunneling via pairs of localized states.[10] The low-temperature value $x \sim 1.2-1.4$ observed for samples S2, S4, and S5 indicates that inelastic tunneling via localized states is the dominant transport mechanism at low temperatures in the samples studied here. Including direct and indirect tunneling processes the conductivity can be written as $G = G_0 + G_0' V^2 + G_1 + G_2 V^{4/3} + \cdots$, where G_n, G_n' denote the coefficients for tunneling via n localized states. The analysis of the conductance of samples S2 and S5 shows that tunneling via impurity states vanishes close to T_C [see Fig. 5(b)] leaving only the small direct tunneling contribution above T_C. Sample S3 has a lower conductance exponent than the theoretical value $x = 4/3$. However, the mechanically induced grain boundary S3 consists of a 50 μm wide disordered region that might contain many tunneling junctions and shunt resistances influencing the determination of the exponent x. The simultaneous decrease of the low-field magnetoresistance and conductance exponent observed for the step-edge array S2 at low temperature is probably due to the transition of the barrier layer to a metallic state.

The anisotropic magnetoresistance (AMR) defined by

$$\mathrm{AMR} = [R_\parallel - R_\perp]/R_{max} \tag{3}$$

was measured for samples S1–S4. $R_\parallel$ and $R_\perp$ denote the resistances measured in longitudinal and transverse current-magnetic field geometry, respectively. Since the measurements were performed on square samples in magnetic fields oriented parallel to the film, demagnetizing effects are supposed to be small. The AMR determined at $\mu_0 H = 0.2$ T is shown in Fig. 6. All investigated samples show AMR values of the same sign and order of magnitude. This is surprising, since the resistance of samples S2–S4 is dominated by grain-boundary transport; thus, one has to conclude that the tunneling barriers show anisotropic magnetoresistance and that the mechanism is the same as in the bulk. Ziese and Sena[5] developed a simple atomic model to explain the AMR observed in LCMO films; they found that the AMR can be semiquantitatively understood using an expression that contains only the local parameters: spin-orbit coupling, and crystal-field and exchange-field splitting. The observed AMR indicates that the charge carriers tunnel via manganese atoms. It is likely that the local environment of the manganese in the barrier is not drastically changed compared to the bulk and an AMR value of the same sign and order of magnitude results in both cases.

I propose the following model to explain the data. In polycrystalline samples at low temperatures transport is dominated by inelastic tunneling through a magnetic barrier between highly spin-polarized, ferromagnetic grains. The charge carriers tunnel via one or two manganese atoms in the barrier. The steep decrease in the resistance observed at low magnetic fields is due to remagnetization processes of the grain magnetization from random orientation to parallel alignment. It is often observed that the measured low-field magnetoresistance is considerably smaller and exhibits a much stronger temperature dependence than the ideal value[13] $\Delta R/R_S = 2P_1P_2/(1-P_1P_2)$ for tunneling between ferro-

magnetic grains with spin polarizations P_1, P_2 through a nonmagnetic barrier. This can be qualitatively understood by the inelastic nature of the tunneling process that leads to an apparent polarization loss.[14] The linear high-field magnetoresistance slope is an intrinsic effect of the barrier. Guinea[15] calculated the magnetoconductance for spin-polarized tunneling via a paramagnetic impurity. Generalizing this result by taking into account magnetic correlations in a mean-field approach, yields $\Delta R/R_0 \propto M_{gb}^2$ in the high-field limit and a magnetoresistance slope proportional to $\chi_{gb} M_{gb}$. M_{gb} denotes the grain-boundary magnetization and χ_{gb} the high-field grain-boundary susceptibility. This result is identical to the result obtained by Evetts *et al.* within a different approach.[4] It has been experimentally shown that the grain boundary is a noncollinear ferromagnet;[6] thus a large high-field susceptibility χ_{gb} extending to very high magnetic fields is expected. Evidence for the spin-glass-like nature of the grain boundary comes from resistance-relaxation measurements. In these experiments Ziese *et al.*[16] observed a significant resistance relaxation in the manganites after a sudden field change; the relaxation strength scales with the low-field magnetoresistance and is therefore a grain-boundary effect. The resistance was observed to depend logarithmically on time suggesting that the grain boundary is a spin glass.

In summary I have reported resistance, magnetoresistance, and dynamic conductance measurements on various LCMO samples. A model of spin-polarized inelastic tunneling through a spin-glass-like barrier is proposed to interpret the data.

This work was supported by the European Union TMR ''OXSEN'' network.

[1] H. Y. Hwang, S-W. Cheong, N. P. Ong, and B. Batlogg, Phys. Rev. Lett. **77**, 2041 (1996).

[2] A. Gupta, G. Q. Gong, Gang Xiao, P. R. Duncombe, P. Lecoeur, P. Trouilloud, Y. Y. Wang, V. P. Dravid, and J. Z. Sun, Phys. Rev. B **54**, R15 629 (1996).

[3] J. M. D. Coey, Philos. Trans. R. Soc. London, Ser. A **356**, 1519 (1998).

[4] J. E. Evetts, M. G. Blamire, N. D. Mathur, S. P. Isaac, B.-S. Teo, L. F. Cohen, and J. L. MacManus-Driscoll, Philos. Trans. R. Soc. London, Ser. A **356**, 1593 (1998).

[5] M. Ziese and S. P. Sena, J. Phys.: Condens. Matter **10**, 2727 (1998).

[6] Ll. Balcells, J. Fontcuberta, B. Martínez, and X. Obradors, Phys. Rev. B **58**, R14 697 (1998).

[7] M. Ziese, G. Heydon, R. Höhne, P. Esquinazi, and J. Dienelt, Appl. Phys. Lett. **74**, 1481 (1999).

[8] C. Srinitiwarawong and M. Ziese, Appl. Phys. Lett. **73**, 1140 (1998).

[9] L. Mieville, D. Worledge, T. H. Geballe, R. Contreras, and K. Char, Appl. Phys. Lett. **73**, 1736 (1998).

[10] L. I. Glazman and K. A. Matveev, Zh. Éksp. Teor. Fiz. **94**, 332 (1988) [Sov. Phys. JETP **67**, 1276 (1988)].

[11] J. G. Simmons, J. Appl. Phys. **34**, 1793 (1963).

[12] M. A. Bari, O. Cabeza, L. Capogna, P. Woodall, and C. M. Muirhead, IEEE Trans. Appl. Supercond. **7**, 2304 (1997).

[13] M. Julliere, Phys. Lett. A **54**, 225 (1975).

[14] E. Yu. Tsymbal and D. G. Pettifor, Phys. Rev. B **58**, 432 (1998).

[15] F. Guinea, Phys. Rev. B **58**, 9212 (1998).

[16] M. Ziese, C. Srinitiwarawong, and C. Shearwood, J. Phys.: Condens. Matter **10**, L659 (1998).